Journal of Medicinal Chemistry

Article

pubs.acs.org/jmc

Arene–Ruthenium(II) Acylpyrazolonato Complexes: Apoptosis-Promoting Effects on Human Cancer Cells

Riccardo Pettinari,*[,†] Claudio Pettinari,[†] Fabio Marchetti,[#] Brian W. Skelton,[ϕ] Allan H. White,[§] Laura Bonfili,[‡] Massimiliano Cuccioloni,[‡] Matteo Mozzicafreddo,[‡] Valentina Cecarini,[‡] Mauro Angeletti,[‡] Massimo Nabissi,[†] and Anna Maria Eleuteri[‡]

[†]School of Pharmacy, [#]School of Science and Technology, and [‡]School of Biosciences and Biotechnology, University of Camerino, via S. Agostino 1, 62032 Camerino, Italy

[§]School of Chemistry and Biochemistry M313 and [ϕ]Centre for Microscopy, Characterization and Microanalysis M010, The University of Western Australia, Crawley, WA 6009, Australia

Supporting Information

ABSTRACT: A series of ruthenium(II) arene complexes with the 4-(biphenyl-4-carbonyl)-3-methyl-1-phenyl-5-pyrazolonate ligand, and related 1,3,5-triaza-7-phosphaadamantane (PTA) derivatives, has been synthesized. The compounds have been characterized by NMR and IR spectroscopy, ESI mass spectrometry, elemental analysis, and X-ray crystallography. Antiproliferative activity in four human cancer cell lines was determined by MTT assay, yielding dose- and cancer cell line-dependent IC_{50} values of 9–34 μM for three hexamethylbenzene–ruthenium complexes, whereas the other metal complexes were much less active. Apoptosis was the mechanism involved in the anticancer activity of such compounds. In fact, the hexamethylbenzene–ruthenium complexes activated caspase activity, with consequent DNA fragmentation, accumulation of pro-apoptotic proteins (p27, p53, p89 PARP fragments), and the concomitant down-regulation of antiapoptotic protein Bcl-2. Biosensor-based binding studies indicated that the ancillary ligands were critical in determining the DNA binding affinities, and competition binding experiments further characterized the nature of the interaction.

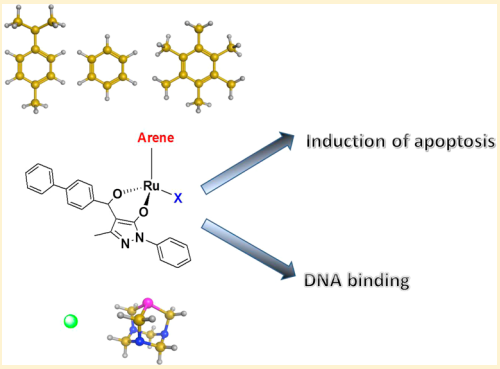

INTRODUCTION

One of the major medical breakthroughs for metal-based drugs was the discovery of the potent antitumor activity of cisplatin.[1] In the effort of fighting drug resistance and severe side effects during treatment, which are the major drawbacks,[2] complexes containing metals other than platinum have become the focus of research.[3] Among the other numerous metal complexes explored for anticancer activity, those of ruthenium occupy a prominent position;[4] two of them, namely NAMI-A[5] and KP1019,[6] having entered phase II clinical trials. Ruthenium(III) complexes are likely to be activated by reduction to Ru(II) in the body and a range of highly active organometallic Ru(II) anticancer complexes have been recently developed by Dyson[7] and Sadler.[8] The structures of their Ru(II) half-sandwich complexes allow for variation of their three main building blocks, the arene, the bidentate ligand, and the monodentate ligand, in fine-tuning their biological properties.[9] The activity of ruthenium arene complexes containing the chelating ligand ethylenediamine, for example $[(\eta^6\text{-arene})Ru(en)Cl]^+$, has been shown to be highly dependent on the nature of the bound arene, with increasing hydrophobicity correlating with increasing cytotoxicity,[10] although further studies have demonstrated that the structure–activity relationship is more complex.[11]

In the "RAPTA" compounds, a class of organometallic ruthenium(II) arene complexes containing the PTA ligand, variation of the arene ligand has shown both *p*-cymene and benzene derivatives to be slightly less cytotoxic than the complex with hexamethylbenzene.[12]

We have previously reported a study on the coordination chemistry of ruthenium arene fragments with unsymmetrical β-diketones containing a pyrazole ring fused to the *O*,*O*′-chelating moiety.[13] In this paper, we report the preparation and characterization of some ruthenium arene complexes containing the 4-(biphenyl-4-carbonyl)-3-methyl-1-phenyl-5-pyrazolonato ligand, with an associated series of biological tests, performed for the first time using this class of metal complexes. The cytotoxicity of arene and ancillary ligands coordinated to ruthenium has been investigated against cervical carcinoma (HeLa), breast adenocarcinoma (MCF-7), hepatocarcinoma (HepG2), and colorectal carcinoma (HCT-116) human cell lines, and the molecular mechanisms beneath the observed effects have been evaluated and dissected.

RESULTS AND DISCUSSION

The pro-ligand HQ^{biph} was synthesized as previously reported.[14] The novel ruthenium arene complexes **1**–**3** were prepared in high yield from the reaction of the appropriate dimer,

Received: October 30, 2013

   dx.doi.org/10.1021/jm500458c | J. Med. Chem. XXXX, XXX, XXX–XXX

Scheme 1

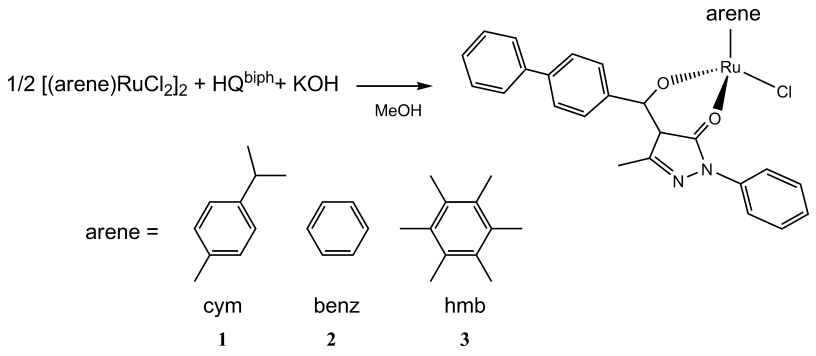

Scheme 2

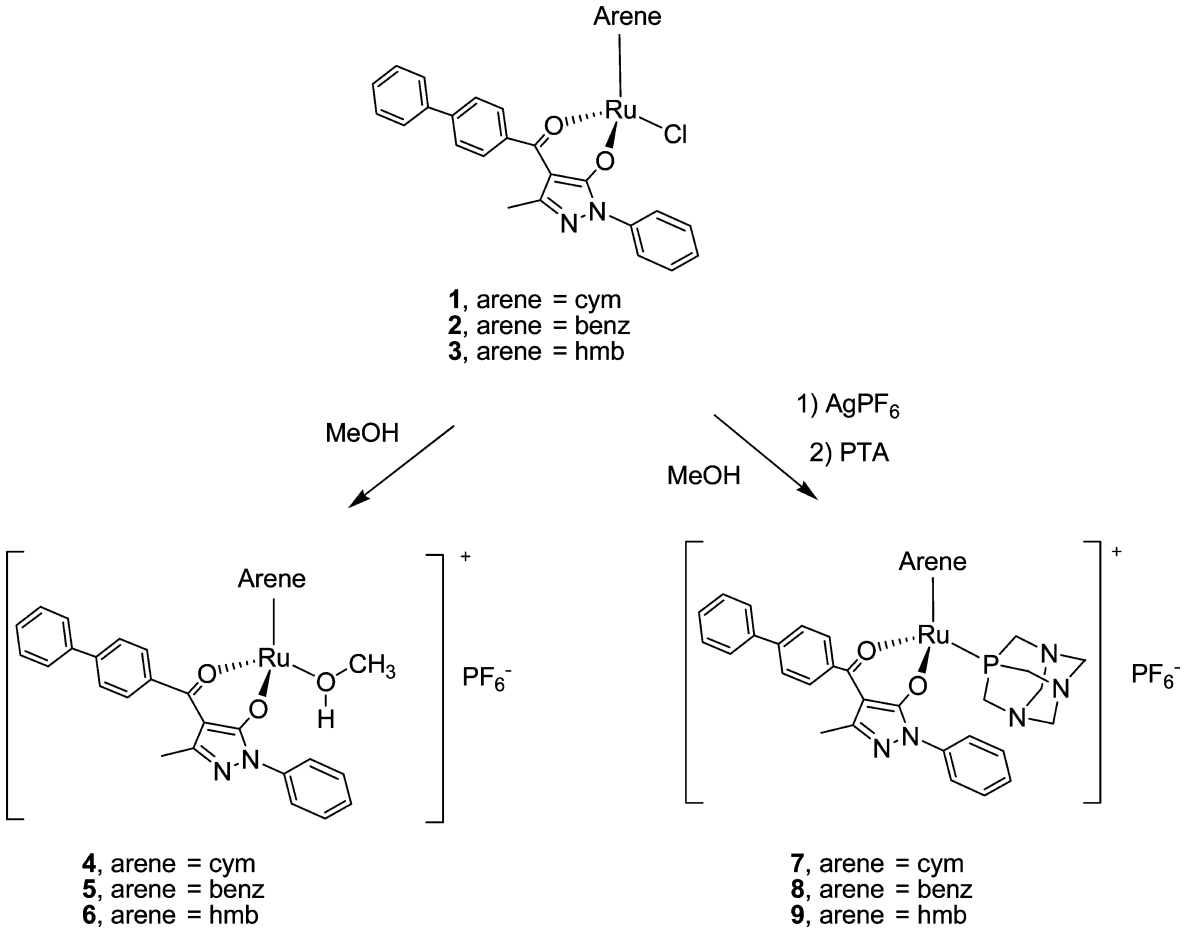

$[(arene)RuCl_2]_2$ (arene = cym (**1**); benz (**2**); hmb (**3**)) with HQ^{biph} and KOH in methanol (Scheme 1). The complexes are air-stable in solution and in the solid-state; they are highly soluble in most organic solvents and sparingly soluble in water. The IR spectra of **1**–**3** show the typical shift of their ν(C=O) vibrations to lower frequency consequent on coordination of the acylpyrazolone ligand to the metal ion.[15] In the positive ESI mass spectra of **1**–**3**, peaks due to the cationic fragment $[(arene)Ru(Q^{biph})]^+$, generated from loss of Cl^-, are observed as the predominant species.

The ^{1}H NMR and ^{13}C NMR spectra of **1**–**3** display distinct shifts of the resonances of the acylpyrazolone protons in comparison with the equivalent protons in the free pro-ligand.

The chloride ligands in **1**, **2**, and **3** can be easily removed by their metathesis reaction with $AgPF_6$ in methanol, to afford $[(cym)Ru(Q^{biph})(CH_3OH)][PF_6]$ (**4**), $[(benz)Ru(Q^{biph})(CH_3OH)][PF_6]$ (**5**), and $[(hmb)Ru(Q^{biph})(CH_3OH)][PF_6]$ (**6**), wherein one methanol molecule supplants the chloride in the ruthenium coordination sphere. The labile methanol molecule in each of **4**, **5**, and **6** can also be replaced by the water-soluble phosphine 1,3,5-triaza-7-phosphaadamantane, affording the complexes $[(cym)Ru(Q^{biph})(PTA)][PF_6]$ (**7**), $[(benz)Ru(Q^{biph})(PTA)][PF_6]$ (**8**), and $[(hmb)Ru(Q^{biph})(PTA)][PF_6]$ (**9**), as depicted in Scheme 2.

Complexes **4**–**9** are soluble in alcohols, acetonitrile, DMSO, and acetone, sparingly soluble in water, and poorly soluble in chlorinated solvents. In acetonitrile, complexes **4**–**9** display conductivity values within the range typical of 1:1 electrolytes.[16] In the IR spectra of derivatives **4**–**9** strong sharp absorptions are

dx.doi.org/10.1021/jm500458c | J. Med. Chem. XXXX, XXX, XXX–XXX

observed at 825 and 830 cm^{-1} arising from their PF_6^- counteranions.[17]

The ^1H NMR spectra of **7**, **8**, and **9** show all the expected signals due to the coordinated arene ring, acylpyrazolone, and PTA, two types of methylene protons being detected for the coordinated PTA ligand. The ^{31}P NMR spectra of **4**–**9** contain a septet ca. −143 ppm, typical of an ionic PF_6^-, and those of **7**, **8**, and **9** exhibit single resonances at −29, −26, and −35 ppm, respectively, due to the PTA ligand, in the region typical of related complexes, and in accordance with the existence of only one species in solution.[17] In the positive ESI mass spectra of **7**–**9**, peaks arising from the cationic fragment $[(arene)Ru(Q^{biph})(PTA)]^+$, generated from the coordination of PTA, are observed as the predominant species.

Structure Determinations. "Low"-temperature (ca. 100 K) single-crystal X-ray structure determinations are recorded for complexes (**1**–**3**) $[(arene)Ru(Q^{biph})Cl]$, and the parent pro-ligand HQ^{biph}, all except the latter being to some degree solvated (Table S1, Supporting Information). In all except **1**, a single molecule (plus solvent, as appropriate), devoid of crystallographic symmetry, comprises the asymmetric unit of the structure; in **1**, two such molecules. In **1**, there is a single molecule of methanol, hydrogen-bonding to the chlorine atom of molecule 1 (rather than displacing it, as in **6**) (Table S2, Supporting Information); in **2** and **3**, in each case a phenyl ring (15× in **2**, 1× in **3**) was modeled as rotationally disordered about the pendant bond over a pair of sites, solvent occupancy being concerted with that of the minor component. Figure 1b shows a projection of **3**

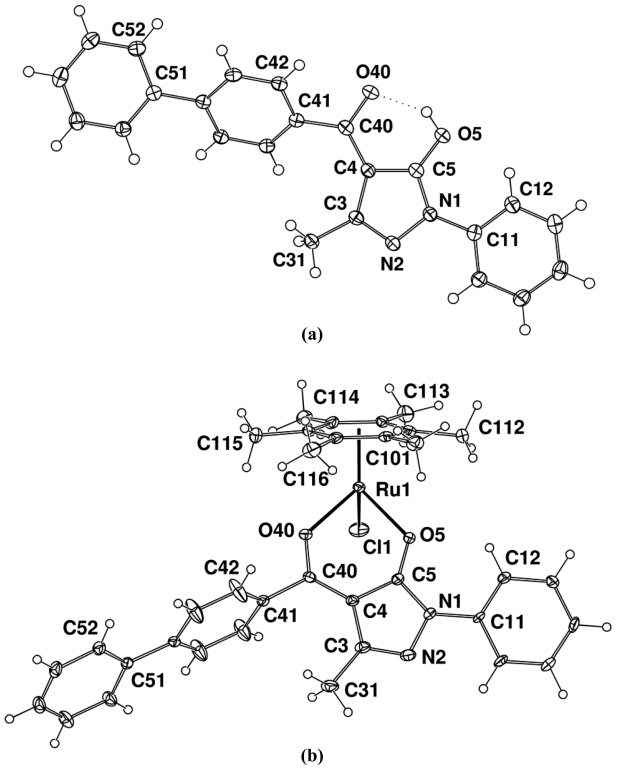

Figure 1. (a) Projection of a molecule of the pro-ligand HQ^{biph} normal to its plane; (b) projection of a single molecule of **3** $[(hmb)Ru(Q^{biph})Cl]$ (major component; pendant phenyl ring 1 is disordered).

as representative of the three complexes, and Figure 1a the pro-ligand. Molecular dimensions and conformational descriptors are given extensively in the summary Table S2, Supporting Information.

The single-crystal studies of **1**–**3** confirm the overall stoichiometry and the mononuclear nature and the quasioctahedral (considering the arene-donor as η^3) coordination environment, about each ruthenium atom, similar to those recorded in numerous other studies.[13] With modification of the arene-donor as the only difference between the three complexes, consequent differences in dimensions are trivial. The Ru–C(0)(arene-centroid) distances are $1.62_9/1.64_6$, 1.63_8, 1.65_2 Å, with that line having a maximum angle of 0.33(14)° between it and the normal to the ligand plane, suggesting little or no difference in whatever interaction there may be between the arene-ligand and the remainder of the substituents, but with considerable conformational differences between the diverse ligands within the one complex (**1**) and between them (**1**–**3**), where all interplanar dihedral angles associated with the pendants now vary widely.

Considerable differences are found in counterpart dimensions between the free pro-ligand HQ^{biph} (which is in the enol form) and those of the complexed form in **1**–**3**, concomitant on replacement of the protonic hydrogen atom by the ruthenium atom, most notably in the O···O bite distance which increases from 2.4815(13) Å in the free ligand to 2.906(6)–2.942(3) Å in the complexes. Changes in the other distances are less notable, but changes of 5° or more are found in those angles forming the chelate ring.

The pro-ligand itself, HQ^{biph} (Figure 1a), is quite closely planar except for a twist of the "inner" ring of the biphenyl pendant of ca. 38° (Table S2, Supporting Information), notwithstanding intercomponent hydrogen contacts which in many cases lie snugly at or just below their van der Waals sums; in **3**, the biphenyl interplanar dihedral angle is as small as 9.4(2)°. The crystal packing is interesting with the molecules lying in sheets normal to *a*, made up of strings of quasiherringbone dispositions within each sheet.

Effect on Cancer Cells. All the compounds were tested (see Experimental Section for details) for their in vitro anticancer activity against cervical carcinoma (HeLa), breast adenocarcinoma (MCF-7), hepatocarcinoma HepG2, and colorectal carcinoma HCT-116 human cell lines (Table 1).

Table 1. Cytotoxicity (IC_{50}, μM) of HQ^{biph} and Complexes 1–9 in Human HeLa, MCF-7, HepG2, and HCT-116 Cancer Cell Lines (n.e.: no effect)

compound	HeLa	MCF-7	HepG2	HCT-116
HQ^{biph}	n.e.	n.e.	n.e.	n.e.
1	n.e.	n.e.	32 ± 3	>100
2	>100	n.e.	30 ± 1	31 ± 4
3	13 ± 3	26 ± 4	28 ± 2	30 ± 6
4	50 ± 7	n.e.	38 ± 3	>100
5	84 ± 5	56 ± 8	35 ± 2	>100
6	25 ± 3	24 ± 2	32 ± 6	34 ± 3
7	>100	88 ± 9	40 ± 3	38 ± 4
8	>100	n.e.	30 ± 5	>100
9	14 ± 2	13 ± 1	27 ± 6	9 ± 3
cisplatin	13[18]	7[18]	12[18]	52[19]

The HQ^{biph} pro-ligand was always totally ineffective against all cancer cell lines. However, the nature of the arene ring plays a major role in establishing the anticancer potency of the ruthenium compounds. In fact, both cancer cell lines tested were particularly sensitive only to hmb-conjugated **3**, **6**, and **9** at 24 h, with IC_{50} values in the range 10–30 μM, whereas benzene- and

dx.doi.org/10.1021/jm500458c | J. Med. Chem. XXXX, XXX, XXX–XXX

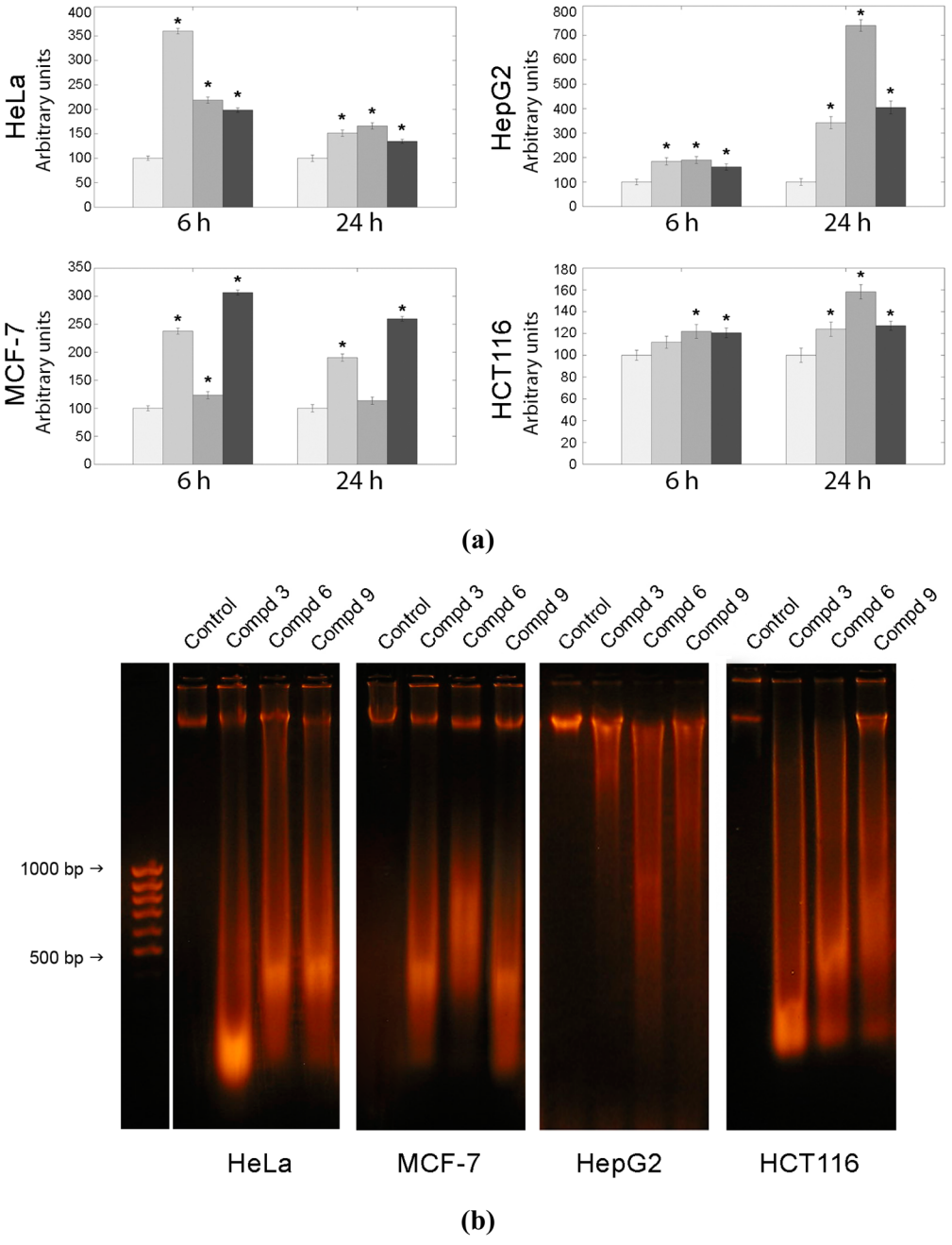

Figure 2. (a) DEVDase activity; (b) DNA fragmentation assay at 24 h. Plots and 1.8% agarose gels stained with EtBr are representative of three separate experiments.

cymene-counterparts generally induced minor, cell line-dependent effects.

Among the cell lines tested, HepG2 cells were in general the most sensitive to all the treatments, as IC_{50} values in the range 27−40 μM were observed. HeLa cells were negligibly affected by the cymene and benzene complexes, with only the CH_3OH ancillary ligand contributing to partial enhancement of the cell-killing effect of the cymene and benzene compounds. Also MCF-7 cells were generally resistant to cymene and benzene compounds over the range of concentration tested, only the benzene−CH_3OH combination (compound **5**) inducing a significant effect. HCT-116 cell model showed the highest degree of sensitivity to compound **9**, also being significantly affected by compounds **2**, **3**, **6**, and **7**.

On the basis of these results, cells were then treated with compounds **3**, **6**, and **9** (those showing the highest cytotoxicity) to explore their ability to activate the apoptotic pathway. In detail, cells were exposed to these compounds for 6 and 24 h and the apoptotic pathway was explored.

Apoptotic Events. Caspase (DEVDase) activity was measured to elucidate the basis for the observed induction of cellular death, as it plays a central role in the execution of the apoptotic program.[20] Its activity was significantly enhanced in all cell lines tested, being clear at 6 h for HeLa and MCF-7 cells, and more evident at 24 h for HepG2 and HCT116 (Figure 2a).

In detail, at 6 h, caspase activity in HeLa cells was similarly up-regulated by all the tested compounds (2- to 2.5-fold increases were observed). Differently, caspase was strongly activated by **3** and **9** in MCF-7 cells. Compound **6** was the most effective in HepG2 and HCT-116 cells.

dx.doi.org/10.1021/jm500458c | J. Med. Chem. XXXX, XXX, XXX−XXX

Late events of apoptosis include DNA cleavage, resulting in the formation of a "ladder" visualized by agarose gel electrophoresis (Figure 2b). DNA fragmentation assay confirmed the progression of apoptosis in all cell types upon 24 h treatment with compounds **3**, **6**, and **9**, consequent on caspase-3 activation and with the fragmentation extent in line with the degree of caspase activation.

Caspases-3 and -7 are primarily responsible for the cleavage of poly(ADP-ribose)polymerase protein (PARP) early during apoptosis. PARP is a nuclear enzyme and catalyzes the poly(ADP-ribosyl)ation of several nuclear proteins using NAD as substrate. During apoptosis, caspase-3-mediated PARP cleavage inactivates the enzyme by destroying its ability to respond to DNA strand breaks.[20] PARP processing by caspases generates an 89 kDa C-terminal fragment. The results on the induction of caspase (DEVDase) activity display a corresponding time- and cell- dependent increase in the levels of the 89 kDa PARP fragment in all cell lines (Figure 3).

To further confirm the activation of apoptosis, we investigated two additional markers of this death pathway, namely proteins p27 and p53. p27/Kip1 protein has been shown to play an important role in human cancer cell apoptosis. MCF-7 cells showed its highest increase in the presence of **3** and **9** after 24 h exposure, whereas a 3- to 4-fold increase was evident at 6 h and persisted up to 24 h for all compounds in HeLa, HepG2, and HCT-116 cell lines.

Regarding the transcription factor p53, its activation and accumulation occur in response to DNA damages, thus leading to cell cycle arrest or apoptosis.[21] We observed the up-regulation of p53 protein in MCF-7 at short exposure time to **3** and **9** and to all compounds in both HepG2 and HCT-116 cells, respectively. Conversely, increased p53 levels were observed in HeLa cells at 24 h exposure to compound **6**.

Bcl-2 is an intracellular membrane-associated oncogene responsible for extending cellular survival.[22] The down-regulation of its expression levels upon treatment with compounds **3**, **6**, and **9** in all cell models considered further confirmed that cell death occurred via apoptosis.

Cell Cycle Analysis. The effects on cell cycle progression of compounds **3**, **6**, and **9** at 8 and 16 h post-treatments, were analyzed in all cell lines. The results showed differential effects on cell cycle phases at 16 h. In particular, we observed a slight cell accumulation in G2/M phase with compound **3** in HeLa and HepG2 cell lines, with compound **6** in all cell lines, and with compound **9** in HeLa, MCF-7, and HepG2 cell lines, compared to vehicle-treated cells (see Supporting Information).

DNA-Binding Assay. The DNA binding ability of compounds **1**−**9** was evaluated according to a biosensor-based approach. Sensing surfaces were obtained as described in Experimental Section. The procedure was optimized after several experiments based upon the variation of streptavidin concentration and immobilization pH value. A streptavidin concentration value of 200 μg/mL and a value of 5 for the immobilization pH (chosen on the basis of the streptavidin isoelectric point) were found to best suit a good immobilization of the protein without affecting its functional properties. Readout in the range 600 arcsec were obtained: these conditions resulted in the coupling of a "Langmuir" partial monolayer of the capturing macromolecule. These data were adequate to minimize possible steric hindrance or shielding effects, which could affect the analysis. Upon saturation of the streptavidin monolayer with biotinylated dsDNA (3′-CCACCCATACCCTGGTGGATGC-AATGT-5′), binding experiments were carried out at increasing ruthenium compound concentrations, each repeated in triplicate. At any titration step, baseline achievement was assessed before adding new ruthenium compounds, and the regeneration steps were then achieved as described in Experimental Section. Each binding reaction was followed up to equilibrium. The monoexponential kinetics of each ruthenium compound to immobilized DNA were recorded (Figure 4): this behavior was ascribed to the ability of the tested compounds to bind DNA on a single site. To assess the validity of the monophasic model in fitting each time course, a standard F-test procedure was used: the biphasic model was statistically nonsignificant at 95% confidence.[23] All complexes displayed moderate affinity to surface-blocked DNA, with equilibrium dissociation constants in the range 1.7−19 μM (Table 2); **7** and **9** displayed the highest affinity. The nature of the ancillary ligands was critical in determining the DNA binding affinities of the tested complexes, with the compounds ranking in the following order: PTA-conjugated > CH_3OH-conjugated > chloride-conjugated. Conversely, the nature of the arene rings affected the DNA binding ability of the compounds only to a minor extent.

Table 2. Kinetic and Equilibrium Parameters of DNA−Ru Complex Binding

compound	k_{ass} (M^{-1} s^{-1})	k_{diss} (s^{-1})	K_D (μM)
1	4300 ± 800	0.063 ± 0.002	14.7 ± 2.3
2	3050 ± 700	0.058 ± 0.013	19.0 ± 6.1
3	4409 ± 1415	0.047 ± 0.020	10.7 ± 5.7
4	9047 ± 1987	0.035 ± 0.011	3.9 ± 1.5
5	5888 ± 1047	0.051 ± 0.010	8.7 ± 2.3
6	10340 ± 2300	0.062 ± 0.020	6.0 ± 2.3
7	26168 ± 1200	0.037 ± 0.010	1.4 ± 0.4
8	13539 ± 673	0.056 ± 0.010	4.1 ± 0.8
9	24752 ± 1520	0.043 ± 0.007	1.7 ± 0.3

Interestingly, the difference in terms of K_D was mainly attributable to the recognition phase, as the rank of association kinetic constants perfectly matched that of the equilibrium parameters, whereas all dissociation kinetics were generally comparable within experimental error (Table 2). The binding stoichiometry was 1:1, as calculated from the extent of binding at asymptotically high concentration of each compound (data not shown).

DNA Binding Competition Experiments. To identify the binding site for compounds **1**−**9** on the DNA 30-mer, we performed three distinct competitive binding studies using two established DNA binders, namely DAPI (4′,6-diamidino-2-phenylindole dihydrochloride) and methyl green, and a DNA intercalator, namely EtBr. In each case, the competition with a second molecule for binding to DNA would result in the loss of either fluorescence or absorbance of the complexes. Globally, all compounds tested were capable of selectively forming a complex with DNA at the minor groove, as proved by the concentration-dependent decrease in fluorescent intensity of DNA-bound DAPI (see Supporting Information). Conversely, no significant decrease in the absorbance of methyl green−DNA complex was observed. Moreover, four out of the nine compounds, namely compounds **1**, **3**, **4**, and **6**, were able to intercalate DNA, as they significantly decreased the fluorescence intensity of EtBr bound to DNA (although to different extents), indicating the competition with EtBr.

■ CONCLUSIONS

Nine novel ruthenium−arene complexes with the 4-(biphenyl-4-carbonyl)-3-methyl-1-phenyl-5-pyrazolonate ligand have been

dx.doi.org/10.1021/jm500458c | J. Med. Chem. XXXX, XXX, XXX−XXX

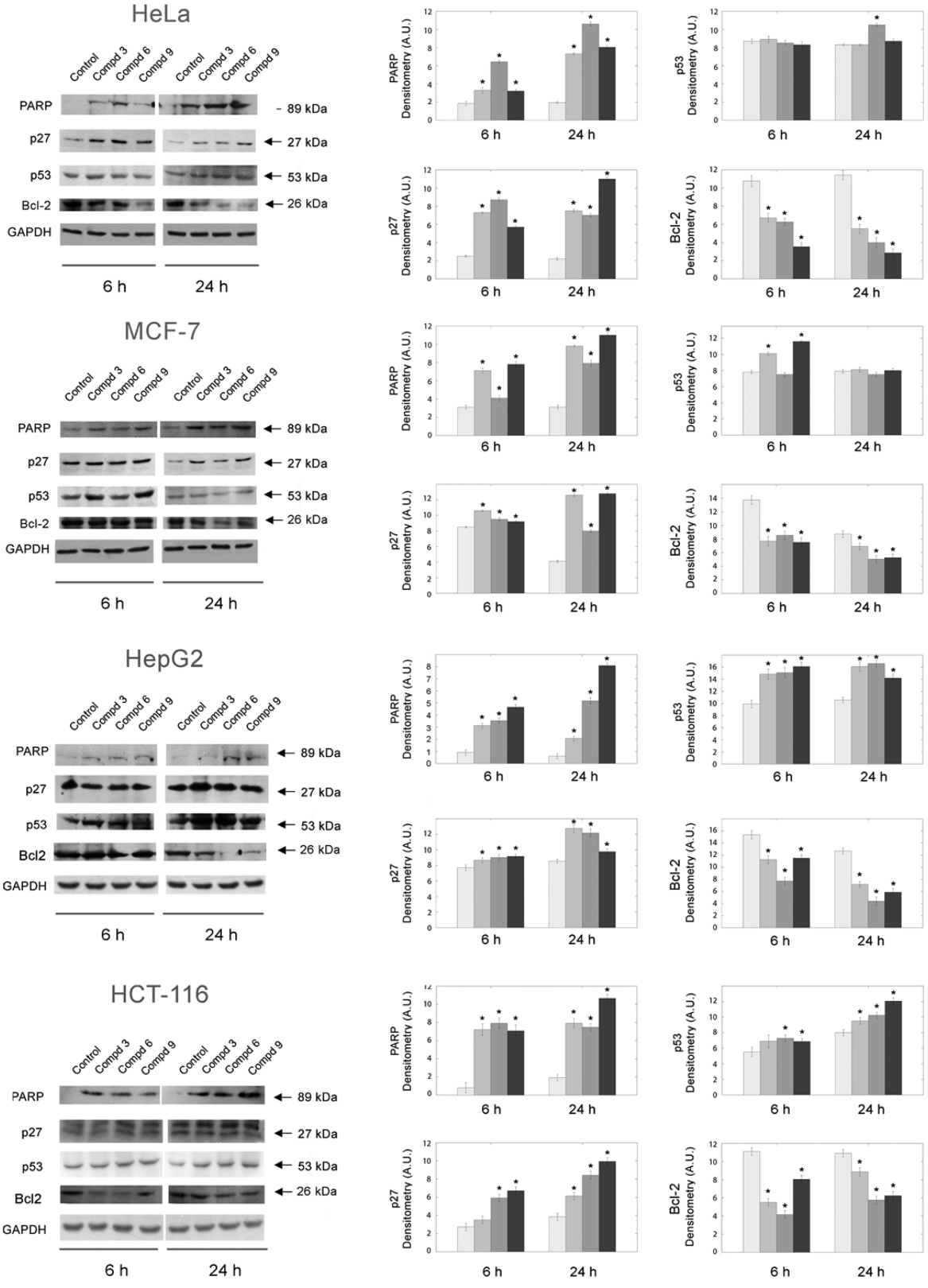

Figure 3. Apoptotic protein markers at 6 and 24 h: autoradiographs of PARP 89 kDa fragment, p27, p53, and Bcl-2 protein levels in HeLa, MCF-7, HepG2, and HCT-116 upon treatment with **3**, **6**, and **9** (representative Western blots are shown). The densitometric analyses from five separate blots provided for quantitative analysis are presented.

synthesized, and the structures have been established by spectroscopic methods together with X-ray diffraction studies. Modification of these Ru(II)−arene complex structures capable of affecting tumor-inhibitory activity in vitro toward four human cancer cell lines (HeLa, MCF-7, HepG2, and HCT116) was investigated. The biological activity of these complexes was

dx.doi.org/10.1021/jm500458c | J. Med. Chem. XXXX, XXX, XXX−XXX

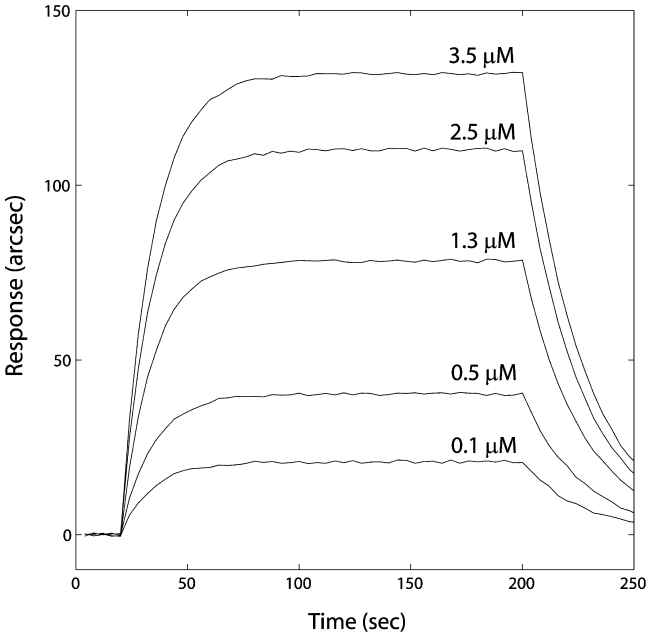

Figure 4. Binding of the ruthenium compounds to DNA. Representative superposition of monoexponential binding curves for compound **2** to surface-blocked DNA 30-mer.

shown to be highly dependent on the nature of the bound arene, the most effective complexes containing hexamethylbenzene as the arene group. Analyzing the IC_{50} values of the compounds, we observed that hexamethylbenzene compounds **3**, **6**, and **9** were particularly active in inducing cell death in all cell lines, with a general potency fully comparable to that previously reported for cisplatin, an approved drug used in the treatment of a number of tumors. Interestingly, upon treatment of HeLa and MCF-7 cells with these most effective molecules, the increase in the caspase DEVDase activity, consequent DNA fragmentation in all cell types, increased expression levels of other downstream proteins involved in the apoptotic pathway, and down-regulation of antiapoptotic protein Bcl-2 were observed. The up-regulation of apoptotic markers was clearly cell type- and compound-dependent, with HeLa, HCT-116, and HepG2 cells being similarly responsive to the three molecules, whereas MCF-7 cells were mainly sensitive to **3** and **9**.

Furthermore, compounds **3**, **6**, and **9** were capable of slightly (but significantly) inducing cell cycle block in G2/M phase in a cell type-dependent manner, probably as a result of DNA intercalation and consistently with the in vitro competitive binding experiments. In fact, besides being all capable of selectively targeting the minor groove of a dsDNA 30-mer with moderate affinity, ruthenium compounds **1**, **3**, **4**, and **6** were also shown to intercalate DNA.

The structures of these ruthenium−arene complexes allow a "twin-track approach": the ancillary ligand determines the DNA binding affinity, whereas the nature of the arene group has a critical role for the apoptosis-based cytotoxicity on the cancer cell types here used. In conclusion, our results demonstrate that chemical modifications of the arene−Ru(II) compound modulate the anticancer activity.

EXPERIMENTAL SECTION

The dimers $[(arene)RuCl_2]_2$ were purchased from Aldrich and TCI Europe and were used as received. The acylpyrazolone pro-ligand HQ^{biph} was synthesized using literature methods.[11] All other materials (products) were obtained from commercial sources and were used as received. IR spectra were recorded from 4000 to 600 cm^{-1} on a PerkinElmer Spectrum 100 FT-IR instrument. ^1H, ^{13}C, and ^{31}P NMR spectra were recorded on a 400 Mercury Plus Varian instrument operating at room temperature (400 MHz for ^1H, 100 MHz for ^{13}C, and 161 MHz for ^{31}P). Referencing is relative to TMS (^1H and ^{13}C) and 85% H_3PO_4 (^{31}P). Positive and negative ion electrospray mass spectra were obtained with a Series 1100 MSI detector HP spectrometer, using an acetonitrile mobile phase. Solutions (3 mg/mL) for electrospray ionization mass spectrometry (ESI-MS) were prepared using reagent-grade acetonitrile. Mass and intensities were compared to those calculated using the IsoPro Isotopic Abundance Simulator, version 2.1.28. Melting points are uncorrected and were taken on an STMP3 Stuart Scientific instrument and on a capillary apparatus. Samples for microanalysis were dried in vacuo to constant weight (20 °C, ca. 0.1 Torr) and were analyzed on a Fisons Instruments 1108 CHNS-O elemental analyzer. Electrical conductivity measurements (Λ_M, reported as S cm^2 mol^{-1}) of acetonitrile and dichloromethane solutions of the complexes were recorded using a Crison CDTM 522 conductimeter at room temperature. Cervical carcinoma (HeLa) and breast adenocarcinoma (MCF-7) human epithelial cell lines were purchased from American Type Culture Collection (ATCC, Manassas, VA). Compound purity was confirmed by elemental analysis with a minimum percentage of 95%.

Synthesis of the Pro-ligand HQ^{biph}. To a hot 1,4-dioxane solution of 1-phenyl-3-methylpyrazol-5-one (4.184 g, 0.024 mol) was added calcium hydroxide (3.556 g, 0.048 mol). The resulting mixture was stirred under reflux for 30 min. Then biphenyl-4-carbonyl chloride (5.00 g, 0.023 mol) was added dropwise to the suspension and the reaction mixture stirred under reflux for 24 h. The brown precipitate formed was treated with 350 mL of 2 M HCl and then filtered off and recrystallized from octane (orange crystals, 80% yield). Mp 148−150 °C. Anal. Calcd for $C_{23}H_{18}N_2O_2$: C, 77.95; H, 5.12; N, 7.90. Found: C, 77.90; H, 5.19; N, 7.84%. IR (cm^{-1}): 3033w, 1606s, 1592s, 1575s, 1534s, 1506m ν(C═C; C═N). ^1H NMR ($CDCl_3$, 298 K): δ, 2.16 (s, 3H, C3-CH_3), 7.26−7.48 (m, 6H), 7.62−7.87 (m, 9H), 10.80 (sbr, 1H, OH). ^{13}C NMR ($CDCl_3$, 298 K): δ, 16.3 (s, C3-CH_3), 103.9 (s, *C*4), 121.0, 129.9, 127.3, 127.5, 128.4, 128.8, 129.2, 129.3, 136.4, 137.4, 140.1, 145.0, 148.1, 161.8, 191.6 (s, ligand). ESI-MS (−) CH_3OH (m/z, relative intensity %): 353 [100] $[Q^{biph}]^-$.

Syntheses of Ruthenium Complexes. *[(cym)Ru(Q^{biph})Cl] (**1**).* To the proligand HQ^{biph} (231.4 mg, 0.652 mmol) dissolved in methanol (20 mL) was added KOH (36.6 mg, 0.652 mmol). The mixture was stirred 1 h at room temperature, and then $[(cym)RuCl_2]_2$ (200.0 mg, 0.326 mmol) was added. The resulting solution was refluxed under stirring for 24 h. The solvent was removed under reduced pressure, and dichloromethane (10 mL) was added. The mixture was filtered to remove sodium chloride. The solution was concentrated to ca. 2 mL and stored at 4 °C. The red crystals obtained and collected (362.5 mg, 0.580 mmol, yield 88%) were soluble in diethyl ether, alcohols, acetone, acetonitrile, DMSO, and chlorinated solvents. Mp 146−148 °C. Anal. Calcd for $C_{33}H_{31}N_2RuClO_2$: C, 63.50; H, 5.01; N, 4.49. Found: C, 63.31; H, 4.89; N, 4.36%. Λ_m (MeCN, 298 K, 10^{-4} mol/L): 24 S cm^2 mol^{-1}. IR (cm^{-1}): 3059w, 1602s, 1591s, 1577s, 1557sh, 1524m ν(C═C; C═N). ^1H NMR ($CDCl_3$, 298 K): δ, 1.38 (d, 3H, ^3J = 7.0 Hz, $CH_3C_6H_4CH(CH_3)_2$), 1.74 (s, 3H, C3-CH_3), 2.26 (s, 3H, CH_3-$C_6H_4CH(CH_3)_2$), 2.97 (sept, 1H, ^3J = 6.9 Hz, $CH_3C_6H_4CH(CH_3)_2$), 5.32 (m, 2H, $CH_3C_6H_4CH(CH_3)_2$), 5.58 (m, 2H, $CH_3C_6H_4CH(CH_3)_2$), 7.20−7.93 (m, 14H, Q^{biph}). ^{13}C NMR ($CDCl_3$, 298 K): δ, 16.7 (s, C3-CH_3), 18.3 (s, $CH_3C_6H_4CH(CH_3)_2$), 22.5 (s, $CH_3C_6H_4CH(CH_3)_2$), 31.0 (s, $CH_3C_6H_4CH(CH_3)_2$), 79.2, 79.3, 82.5, 82.6, 96.9, 99.7 (s, $CH_3C_6H_4CH(CH_3)_2$), 106.6 (s, *C*4), 121.2, 125.5, 126.9, 127.4, 128.1, 128.7, 129.1, 137.7, 138.7, 140.3, 143.6, 149.2, 163.8, 188.0 (s, Q^{biph}). ESI-MS (+) CH_3OH (m/z, relative intensity %): 589 [100] $[(cym)Ru(Q^{biph})]^+$.

*[(benz)Ru(Q^{biph})Cl] (**2**).* The synthesis was performed as for **1** using $[(benz)RuCl_2]_2$ (163.3 mg, 0.326 mmol). **2** is soluble in alcohols, acetone, acetonitrile, DMSO, and chlorinated solvents. Mp 264−266 °C. Anal. Calcd for $C_{29}H_{23}N_2O_2RuCl$: C, 61.32; H, 4.08; N, 4.93. Found: C, 61.01; H,4.16; N, 4.86%. Λ_m (MeCN, 298 K, 10^{-4} mol/L): 18 S cm^2 mol^{-1}.

dx.doi.org/10.1021/jm500458c | J. Med. Chem. XXXX, XXX, XXX−XXX

IR (cm^{-1}): 3051w, 1592vs ν(C═O), 1579s, 1556sh, 1528m ν(C═C; C═N). ^1H NMR ($CDCl_3$, 298 K): δ, 1.71 (s, 3H, C3-CH_3), 5.73 (s, 6H, C_6H_6), 7.22−7.92 (m, 14H, Q^{biph}). ^{13}C NMR ($CDCl_3$, 298 K): δ, 16.6 (s, C3-CH_3), 82.3 (s, C_6H_6), 106.6 (s, *C*4), 121.1, 125.7, 127.0, 127.3, 127.4, 128.1, 128.6, 128.9, 129.2, 137.3, 138.7, 140.3, 143.6, 149.3, 163.4, 188.4 (s, Q^{biph}). ESI-MS (+) CH_3OH (*m*/*z*, relative intensity %): 533 [100] $[(benz)Ru(Q^{biph})]^+$.

*[(hmb)Ru(Q^{biph})Cl] (**3**).* The synthesis was performed as for **1** using $[(hmb)RuCl_2]_2$ (218.3 mg, 0.326 mmol). **3** is soluble in alcohols, acetone, acetonitrile, DMSO, and chlorinated solvents. Mp 295−297 °C. Anal. Calcd for $C_{35}H_{35}N_2O_2RuCl$: C, 64.46; H, 5.41; N, 4.30. Found: C, 64.18; H, 5.43; N, 4.25%. Λ_m (MeCN, 298 K, 10^{-4} mol/L): 13 S cm^2 mol^{-1} IR (cm^{-1}): 3030w, 1602s, 1591s, 1578s, 1539m ν(C═C; C═N). ^1H NMR ($CDCl_3$, 298 K): δ, 1.72 (s, 3H, C3-CH_3), 2.08 (s, 18H, $C_6(CH_3)_6$), 7.17−7.97 (m, 14H, Q_{biph}). ^{13}C NMR ($CDCl_3$, 298 K): δ, 15.2 (s, $C_6(CH_3)_6$), 15.8 (s, C3-CH_3), 92.0 (s, $C_6(CH_3)_6$), 102.2 (s, *C*4), 119.5, 122.0, 124.7, 124.8, 124.9, 126.9, 127.8, 128.3, 128.4, 128.7, 129.0, 129.1, 137.5, 138.6, 140.4, 143.8, 149.1, 163.7, 188.2 (s, Q^{biph}). ESI-MS (+) CH_3OH (*m*/*z*, relative intensity %): 617 [100]$[(hmb)Ru(Q^{biph})]^+$.

*[(cym)Ru(Q^{biph})(CH_3OH)][PF_6] (**4**).* Silver hexafluorophosphate (78.0 mg, 0.312 mmol) was added to a solution of $[(cym)Ru(Q^{biph})Cl]$ (**1**, 184.6 mg, 0.312 mmol) in methanol. The reaction mixture was refluxed for 24 h and then allowed to cool to room temperature. The solvent was removed under reduced pressure, and chloroform (15 mL) was added. The mixture was filtered to remove AgCl, the solution was dried under vacuum, and the red residue was identified as **4** (224.2 mg, 0.298 mmol, 72% yield) which is soluble in alcohols, acetone, acetonitrile, DMSO, and sparingly soluble in chlorinated solvents. Mp 169−171 °C. Anal. Calcd for $C_{34}H_{36}F_6N_2O_3PRu$: C, 53.26; H, 4.73; N, 3.65. Found: C, 53.03; H, 4.53; N, 3.54%. Λ_m (MeCN, 298 K, 10^{-4} mol/L): 130 S cm^2 mol^{-1}. IR (cm^{-1}): 3078w, 1600s, 1576s, 1555hs, 1520m ν(C═C; C═N), 829s ν(PF_6). ^1H NMR (CD_2Cl_2, 298 K): δ, 1.03 and 1.15 (d, 3H, ^3J = 6.8 Hz, $CH_3C_6H_4CH(CH_3)_2$), 1.26 (s, 3H, C3-CH_3), 1.80 (s, 3H, $CH_3C_6H_4CH(CH_3)_2$), 2.13 (sbr, 3H, CH_3OH), 2.45 (m, 1H, $CH_3C_6H_4CH(CH_3)_2$), 4.08 (d, 1H, ^3J = 6.0 Hz, $CH_3C_6H_4CH(CH_3)_2$), 5.60 (d, 2H, ^3J = 6.0 Hz, $CH_3C_6H_4CH(CH_3)_2$), 5.71 (d, 2H, ^3J = 6.0 Hz, $CH_3C_6H_4CH(CH_3)_2$), 5.90 (d, 1H, ^3J = 6.0 Hz, $CH_3C_6H_4CH(CH_3)_2$), 7.21−8.04 (m, 14H, Q^{biph}). ^{13}C NMR ($CDCl_3$, 298 K): δ, 16.7 (s, C3-CH_3), 18.3 (s, $CH_3C_6H_4CH(CH_3)_2$), 22.6 (s, $CH_3C_6H_4CH(CH_3)_2$), 31.1 (s, $CH_3C_6H_4CH(CH_3)_2$), 79.2, 79.3, 82.5, 82.6, 96.9, 99.7 (s, CH_3-C_6H_4−$CH(CH_3)_2$), 106.5 (s, *C*4), 121.2, 121.3, 125.4, 125.9, 126.9, 127.0, 127.5, 128.1, 128.7, 129.1, 137.7, 138.7, 140.3, 143.6, 149.2, 163.8, 188.0 (s, Q^{biph}). ^{31}P NMR ($CDCl_3$, 298 K): δ = −143.2 (sept, PF_6). ESI-MS (+) CH_3OH (*m*/*z*, relative intensity %): 590 [100] $[(cym)Ru(Q^{biph})]^+$.

*[(benz)Ru(Q^{biph})(CH_3OH)][PF_6] (**5**).* The synthesis was performed as for **4** using $[(benz)RuCl_2]_2$ (177.5 mg, 0.312 mmol). **5** is soluble in alcohols, acetone, acetonitrile, and DMSO and sparingly soluble in chlorinated solvents. Mp 230−232 °C. Anal. Calcd for $C_{30}H_{28}F_6N_2O_3PRu$: C, 50.71; H, 3.97; N, 3.94. Found: C, 50.43; H, 3.84; N, 3.98%. Λ_m (MeCN, 298 K, 10^{-4} mol/L): 136 S cm^2 mol^{-1}. IR (cm^{-1}): 3051w, 1592vs ν(C═O), 1580s, 1556sh, 1528m ν(C═C; C═N), 825s ν(PF_6). ^1H NMR (CD_3CN, 298 K): δ, 1.69 (s, 3H, C3-CH_3), 2.01 (2H, H_2O), 5.00 (s, 6H, C_6H_6), 7.22−8.03 (m, 14H, Q^{biph}). ^{13}C NMR ($CDCl_3$, 298 K): δ, 16.6 (s, C3-CH_3), 82.3 (s, C_6H_6), 106.6 (s, *C*4), 121.1, 125.7, 127.0, 127.3, 127.4, 128.1, 128.6, 128.9, 129.2, 137.3, 138.7, 140.3, 143.6, 149.3, 163.4, 188.4 (s, Q^{biph}). ^{31}P NMR ($CDCl_3$, 298 K): δ= −143.3 (sept, PF_6). ESI-MS (+) CH_3OH (*m*/*z*, relative intensity %): 533 [100] $[(benz)Ru(Q^{biph})]^+$.

*[(hmb)Ru(Q^{biph})(CH_3OH)][PF_6] (**6**).* The synthesis was performed as for **4** using $[(hmb)RuCl_2]_2$ (203.7 mg, 0.312 mmol). **6** is soluble in alcohols, acetone, acetonitrile, and DMSO and sparingly soluble in chlorinated solvents. Mp 197−199 °C. Anal. Calcd for $C_{36}H_{39}F_6N_2O_3PRu$: C, 54.47; H, 4.95; N, 3.53. Found: C, 54.18; H, 4.73; N, 3.25%. Λ_m (MeCN, 298 K, 10^{-4} mol/L): 138 S cm^2 mol^{-1}. IR (cm^{-1}): 3030w, 1602s, 1591s, 1578s, 1539m ν(C═C; C═N), 827s ν(PF_6). ^1H NMR ($CDCl_3$, 298 K): δ, 1.73 (s, 3H, C3-CH_3), 2.09 (s, 18H, $C_6(CH_3)_6$), 7.25−7.96 (m, 14H, Q^{biph}). ^{13}C NMR ($CDCl_3$, 298 K): δ, 15.6 (s, $C_6(CH_3)_6$), 16.8 (s, C3-CH_3), 90.0 (s, $C_6(CH_3)_6$), 100.2 (s, *C*4), 121.0, 125.2, 126.8, 127.1, 127.3, 127.4, 128.1, 128.6, 128.7, 128.8, 129.2, 129.3, 138.4, 140.0, 143.0, 149.1, 163.7 (s, Q^{biph}). ^{31}P NMR ($CDCl_3$, 298 K): δ = −143.2 (sept, PF_6). ESI-MS (+) CH_3OH (*m*/*z*, relative intensity %): 617 [100] $[(hmb)Ru(Q^{biph})]^+$.

*[(cym)Ru(Q^{biph})(PTA)][PF_6] (**7**).* $AgPF_6$ (58.3 mg, 0.231 mmol) was added to a solution of $[(cym)Ru(Q^{biph})Cl]$ (144.2 mg, 0.231 mmol) in acetone. The reaction mixture was stirred for 1 h at room temperature, and PTA (36.4 mg, 0.231 mmol) was added. After 24 h, the mixture was filtered to remove AgCl, the solution was dried under vacuum, and the red residue was identified as compound **3** (185.2 mg, 0.208 mmol, 90% yield). It is soluble in diethyl ether, alcohols, acetone, acetonitrile, DMSO, and chlorinated solvents and sparingly soluble in water. Mp 189−191 °C. Anal. Calcd for $C_{39}H_{43}F_6N_5O_2P_2Ru$: C, 51.54; H,4.99; N,7.71. Found: C, 51.05; H, 4.69; N, 7.39%. Λ_m (MeCN, 298 K, 10^{-4} mol/L): 145 S cm^2 mol^{-1}. IR (cm^{-1}): 3062w, 1599s, 1573s, 1555sh, 1534w ν(C═C; C═N), 830s ν(PF_6). ^1H NMR ($CDCl_3$, 298 K): δ, 1.23 (d, 6H, $CH_3C_6H_4CH(CH_3)_2$), 1.90 (s, 3H, C3-CH_3), 1.98 (s, 3H, $CH_3C_6H_4CH(CH_3)_2$), 2.55 (m, 1H, $CH_3C_6H_4CH(CH_3)_2$), 4.21 (s, 6H, PCH^AH^BN, PTA), 4.50 (m, 6H, PTA), 5.92 (d, 4H, $CH_3C_6H_4CH(CH_3)_2$), 7.25−7.83 (m, 14H, Q^{biph}). ^{13}C NMR ($CDCl_3$, 298 K): δ, 16.9 (s, C3-CH_3), 17.6 (s, $CH_3C_6H_4CH(CH_3)_2$), 22.1 and 22.5 (s, $CH_3C_6H_4CH(CH_3)_2$), 31.1 (s, $CH_3C_6H_4CH(CH_3)_2$), 51.3 (d, P-CH_2N, PTA), 73.1 (d, N-CH_2N, PTA), 86.6, 88.0, 88.6, 85.5, 97.6, 103.7 (s, $CH_3C_6H_4CH(CH_3)_2$), 108.2 (s, *C*4), 120.4, 126.7, 127.4, 127.6, 128.7, 129.3, 135.8, 137.8, 139.6, 145.3, 149.2, 163.1, 191.3 (s, Q^{biph}). ^{31}P NMR ($CDCl_3$, 298 K): δ, −29.1; −143.2 (sept, PF_6). ESI-MS (+) CH_3OH (*m*/*z*, relative intensity %): 746 [100] $[(cym)Ru(Q^{biph})$-$(PTA)]^+$.

*[(benz)Ru(Q^{biph})(PTA)][PF_6] (**8**).* The synthesis was performed as for **7** using $[(benz)RuCl_2]_2$ (177.5 mg, 0.312 mmol). **8** is soluble in alcohols, acetone, acetonitrile, DMSO, and chlorinated solvents and sparingly soluble in water. Mp 240−243 °C. Anal. Calcd for $C_{35}H_{36}F_6N_5O_2P_2Ru$: C, 50.30; H, 4.34; N, 8.38. Found: C, 50.06; H, 4.24; N, 8.31%. Λ_m (MeCN, 298 K, 10^{-4} mol/L): 141 S cm^2 mol^{-1}. IR (cm^{-1}): 3053w, 1598s, 1590s, 1572s, 1544s, 1519w ν(C═C; C═N), 827s ν(PF_6). ^1H NMR (CD_3CN, 298 K): δ, 1.82 (s, 3H, C3-CH_3), 4.21 (s, 6H, PCH^AH^BN, PTA), 4.50 (s, 6H, NCH^AH^BN, PTA), 5.90 (s, 6H, C_6H_6), 7.32−7.97 (m, 14H, Q^{biph}). ^{13}C NMR (CD_3CN, 298 K): δ, 16.4 (s, C3-CH_3), 50.7 (d, P-CH_2N, PTA), 72.8 (d, N-CH_2N, PTA), 87.4 (d, C_6H_6), 119.6, 120.8, 125.3, 125.6, 127.0, 127.1, 127.3, 127.7, 127.9, 128.2, 128.3, 128.6, 129.1, 129.3, 135.4, 138.8, 140.2, 142.8, 149.1, 162.21, 190.3 (s, Q^{biph}). ^{31}P NMR (CD_3CN, 298 K):δ, −26.54; −143.3 (sept, PF_6). ESI-MS (+) CH_3OH (*m*/*z*, relative intensity %): 690 [100] $[(benz)Ru(Q^{biph})(PTA)]^+$.

*[(hmb)Ru(Q^{biph})(PTA)][PF_6] (**9**).* The synthesis was performed as for **7** using $[(hmb)RuCl_2]_2$(208 mg, 0.312 mmol). **9** is soluble in alcohols, acetone, acetonitrile, DMSO, and chlorinated solvents and sparingly soluble in water. Mp 215−217 °C. Anal. Calcd for $C_{41}H_{47}F_6N_5O_2P_2Ru$: C, 53.59; H, 5.16; N, 7.62. Found: C, 53.36; H, 5.04; N, 7.41%. Λ_m (MeCN, 298 K, 10^{-4} mol/L): 146 S cm^2 mol^{-1}. IR (cm^{-1}): 3050w, 1595s, 1584s, 1570s, 1540s, 1516w ν(C═C; C═N), 829s ν(PF_6). ^1H NMR ($CDCl_3$, 298 K): δ, 1.90 (s, 3H, C3-CH_3), 2.08 (s, 18H, $C_6(CH_3)_6$), 4.10 (s, 6H, PCH^AH^BN, PTA), 4.48 (s, 6H, NCH^AH^BN, PTA), 7.25−7.87 (m, 14H, Q^{biph}). ^{13}C NMR ($CDCl_3$, 298 K): δ, 15.6 (s, $C_6(CH_3)_6$), 16.2 (s, C3-CH_3), 49.8 (d, P-CH_2N, PTA), 73.2 (d, N-CH_2N, PTA), 97.7 (s, $C_6(CH_3)_6$), 120.6, 120.9, 125.2, 126.8, 127.5, 127.7, 128.6, 129.1, 129.3, 129.4 (s, Q^{biph}). ^{31}P NMR (CD_3CN, 298 K):δ, −35.7; −143.2 (sept, PF_6). ESI-MS (+) CH_3OH (*m*/*z*, relative intensity %): 774 [100] $[(hmb)Ru(Q^{biph})(PTA)]^+$.

Structure Determinations. Full spheres of "low"-temperature (100 K) CCD area-detector diffractometer data were measured (monochromatic Mo Kα radiation (λ = 0.7107$_3$ Å), ω-scans) yielding N_{total} reflections, these merging to *N* unique (R_{int} cited), after analytical (**1**−**3**) or "empirical"/multiscan (HQ^{biph}) absorption correction, which were used in the full matrix least-squares refinements on F^2, refining anisotropic displacement parameter forms for the non-hydrogen atoms, hydrogen atom treatment following a riding model (reflection weights: $(\sigma^2(F_o^2) + (aP)^2 + (bP))^{-1}$ $(P = (F_o^2 + 2F_c^2)/3)$); N_0 with $I > 2\sigma(I)$ were considered "observed". Neutral atom complex scattering factors were used within the SHELXL97 program.[24] Pertinent results are given below and in the tables and figures, the latter showing 50% probability amplitude displacement envelopes for the non-hydrogen atoms, hydrogen

dx.doi.org/10.1021/jm500458c | J. Med. Chem. XXXX, XXX, XXX−XXX

atoms having arbitrary radii of 0.1 Å. Full cif depositions (excluding structure factors) lodged with the Cambridge Crystallographic Data Centre [CCDC 942931 (for HQ^{biph}), 942932 (for **1**), 942933 (for **2**), 942934 (for **3**)] contain the supplementary crystallographic data for this paper. These data can be obtained free of charge from The Cambridge Crystallographic Data Centre via www.ccdc.cam.ac.uk/data_request/cif.

Cell Viability Assays. Cells were grown in a 5% CO_2 atmosphere at 37 °C in 100 mm tissue culture dishes. Growth media were D-MEM supplemented with 10% FBS, antibiotic, and antimycotic for HeLa cells, and MEM supplemented with 10% FBS, 1% sodium pyruvate, antibiotic, and antimycotic for MCF-7 and HepG2. HCT-116 were grown in RPMI supplemented with 10% FBS. Media and reagents for cell culture were purchased from EuroClone S.p.A. (Milan, Italy).

The effect of arene−Ru derivatives on HeLa, MCF-7, HepG2, and HCT-116 cells viability was determined by 3-(4,5-dimethylthiazol-2-yl)-2,5-diphenyltetrazolium bromide (MTT) assay.[25] After individual treatments with compounds **1**−**9**, MTT was added to the culture medium at a final concentration of 0.5 mg/mL and incubated for 2 h at 37 °C. The medium was replaced with 100 μL of DMSO, and the optical density was measured at 550 nm after 10 min on a microplate reader. At least six cultures were used for each time point.

Cell Treatment. Cells were treated for 6 and 24 h with compounds **3** (30 μM), **6** (30 μM), and **9** (15 μM). Upon treatment, cells were harvested in PBS and centrifuged, and the pellet was dispersed in a lysis buffer (20 mM Tris, pH 7.4, 250 mM sucrose, 1 mM EDTA, and 5 mM β-mercaptoethanol) and passed through a 29-gauge needle at least 10 times. Lysates were centrifuged at 12 000*g* for 15 min, and the supernatants were stored at −80 °C. Protein concentration in cell lysates was determined by the Bradford method[26] using bovine serum albumin as standard.

Caspase Activity Assay. Caspase-3 and -7 (DEVDase) activity assays were performed in cell lysates (5 μg of total proteins in the mixture) using the Ac-Asp-Glu-Val-Asp-AMC substrate (Sigma-Aldrich S.r.L., Milan, Italy) in 50 mM Tris-HCl, 50 mM NaCl, 5 mM $CaCl_2$, 1 mM EDTA, 0.1% CHAPS, 5 mM β-mercaptoethanol, pH 7.5. The incubation was carried out at 37 °C for 60 min, and the hydrolysis product was detected (AMC: λ_{exc} = 365 nm, λ_{em} = 449 nm) on a SpectraMax Gemini XPS microplate reader.

DNA Fragmentation Assay. An amount of 1×10^6 cells was grown in six-well microtiter plates; upon 24 h treatment with compounds **3** (30 μM), **6** (30 μM), and **9** (15 μM), the Buonnano et al. procedure[27] was followed: cells were collected and the pellets were suspended in lysis buffer (50 mM Tris-HCl pH 8, 10 mM EDTA, 0.5% SDS, and 0.5 mg/mL proteinase K). After 1 h incubation at 50 °C, 10 mg/mL RNase was added to the lysates and incubated for 1 h at 50 °C and for 10 min at 70 °C. DNA was precipitated with NaOAc pH 5.2 and ice-cold 100% EtOH, incubated on ice for 10 min, and centrifuged at 10 000*g* for 10 min. Pellets were dissolved in sterile water. Samples were resolved on a 1.8% agarose gel stained with ethidium bromide.

Western Blotting Analyses. Western Blotting assays were performed to analyze intracellular levels of the apoptotic markers poly(ADP-ribose) polymerase (PARP), p27, p53, and Bcl-2 following treatment with the hmb-bearing compounds **3**, **6**, and **9**. Primary and secondary antibodies were obtained from Santa Cruz Biotech (Heidelberg, Germany). Cell lysates (20 μg) were loaded on 12% SDS-PAGE (10% for PARP) and electroblotted onto PVDF membranes Millipore (Milan, Italy). After incubation with primary antibodies, the immunoblot detections were carried out with the Enhanced ChemiLuminescence Western Blotting analysis system (Amersham-Pharmacia-Biotech). Every gel was loaded with molecular weight markers including proteins from 6.5 to 205 kDa. As a control for equal protein loading, glyceraldehyde-3-phosphate dehydrogenase (GAPDH) was utilized: membranes were stripped and reprobed for GAPDH using a monoclonal antibody diluted 1:500. A previously described densitometric algorithm was used to quantitate the Western Blot results.[28]

Cell Cycle Analysis. For these analysis, 3×10^5 cells/mL were incubated with compounds **3**, **6**, and **9** for 8 and 16 h. Upon incubation, cells were fixed for 1 h by adding ice-cold 70% ethanol and then washed with PBS containing 2% FBS and 0.01% NaN_3. Next, the cells were treated with 10 μg/mL ribonuclease A solution (Sigma-Aldrich), incubated for 30 min at 37 °C, stained for 30 min at room temperature with 20 μg/mL of propidium iodide (Sigma-Aldrich), and finally analyzed by flow cytometry using linear amplification.

DNA Binding Assay. The abilities of compounds **1**−**9** to bind DNA were tested according to a biosensor-based assay. The carboxylate surface of the biosensor cuvette was washed and equilibrated with PBS buffer (10 mM Na_2HPO_4, 2.7 mM KCl, 138 mM NaCl, pH = 7.4) and then activated by addition of an equimolar mixture of *N*-hydroxysuccinimide and *N*-ethyl-*N*-(dimethylaminopropyl)carbodiimide hydrochloride.[29] Streptavidin was dissolved in 10 mM CH_3COONa buffer (pH 5) and then anchored to the carboxylic surface. Free carboxylic sites on the sensor surface were deactivated by injection of 1 M ethanolamine, pH 8.5. Finally, 5′-biotinylated dsDNA (3′-CCACCCAC-TACCCTGGTTGGATGCTAATGT-5′) was coupled to the streptavidin-coated surface. Compounds **1**−**9** were added to the DNA-functionalized surface at different concentrations, and binding kinetics were routinely followed up to equilibrium. Dissociation steps were performed by a single 1 min wash (80 μL) with fresh PBS buffer, whereas free DNA surface regeneration was achieved by serial PBS washes (the number of washing cycles depending on the interaction strength), each time assessing the recovery of free DNA baseline prior to any further addition of the ruthenium compounds. Raw data were globally fitted to both mono- and biexponential models, and the validity of each model to fit a particular time course was assessed by a standard F-test procedure.

DAPI Displacement Assay. DAPI is a DNA minor groove binder,[30] whose fluorescence intensity is enhanced upon DNA complexation. DAPI displacement was assayed by recording the emission spectra of solutions containing different concentrations of compounds **1**−**9** (0−100 μM), DNA (20 μM), and DAPI (15 μM) in phosphate buffer (10 mM, pH 7.4) at room temperature after excitation at 338 nm on a Gemini XPS microplate reader.

Methyl Green Displacement Assay. Methyl Green is a major groove binder,[31] whose evanescent native UV−vis absorbance is retained in complexes with DNA. Methyl Green was suspended in 50 mM Tris-HCl buffer, pH 7.5, containing 7.5 mM $MgSO_4$ and incubated with DNA (200 μM) for 24 h at 37 °C. Next, the displacement assay was performed by monitoring the absorbance at 630 nm upon addition of candidate competitors (compounds **1**−**9** (100 μM)) with a Bio-Tek Visible plate reader.

EtBr Competitive Binding Assay. EtBr is an established DNA intercalator.[32] EtBr binding assay was performed by monitoring the changes in the emission spectra of solutions containing different concentrations of compounds **1**−**9** (0−100 μM), DNA (20 μM), and EtBr (10 μM) in phosphate buffer (pH 7.4) at room temperature upon excitation at 480 nm on a Gemini XPS microplate reader.

Statistical Analysis. Results are expressed as mean values with their standard deviations obtained from five separate experiments. Statistical analysis was performed with one-way ANOVA, followed by the Bonferroni test using Sigma-stat 3.1 software (SPSS, Chicago, IL). *p*-Values <0.05 and <0.01 were considered to be significant.

■ ASSOCIATED CONTENT

Supporting Information

Tables S1,2 comprising crystal/refinement data and non-hydrogen atom molecular dimensions for HQbiph and compounds **1**−**3**. Fluorescence spectra and absorbance readings of competitive DNA binding experiments. Cell cycle curves obtained by FACS analysis. Crystallographic data in CIF format for HQbiph, **1**−**3**. This material is available free of charge via the Internet at http://pubs.acs.org.

■ AUTHOR INFORMATION

Corresponding Author

*Phone: +39 0737402338. Fax: +39 0737 402338. E-mail: riccardo.pettinari@unicam.it.

Author Contributions

The manuscript was written through contributions of all authors. All authors have given approval to the final version of the manuscript.

Notes

The authors declare no competing financial interest.

■ ACKNOWLEDGMENTS

We thank the University of Camerino for financial support.

■ REFERENCES

(1) (a) Wang, D.; Lippard, S. J. Cellular processing of platinum anticancer drugs. *Nat. Rev. Drug Discovery* **2005**, *4*, 307−320. (b) Wheate, N. J.; Walker, S.; Craig, G. E.; Oun, R. The status of platinum anticancer drugs in the clinic and in clinical trials. *Dalton Trans.* **2010**, *39*, 8113−8127.

(2) Heffeter, P.; Jungwirth, U.; Jakupec, M.; Hartinger, C.; Galanski, M.; Elbling, L.; Micksche, M.; Keppler, B. K.; Berger, W. Resistance against novel anticancer metal compounds: Differences and similarities. *Drug Resist. Updates* **2008**, *11*, 1−16.

(3) (a) Jakupec, M. A.; Galanski, M.; Arion, V. B.; Hartinger, C. G.; Keppler, B. K. Antitumor metal compounds: More than theme and variations. *Dalton Trans.* **2008**, 183−194. (b) Barry, N. P. E.; Sadler, P. J. Exploration of the medical periodic table: Towards new targets. *Chem. Commun.* **2013**, *49*, 5106−5131.

(4) (a) Levina, A.; Mitra, A.; Lay, P. A. Recent developments in ruthenium anticancer drugs. *Metallomics* **2009**, *1*, 458−470. (b) Suss-Fink, G. Arene ruthenium complexes as anticancer agents. *Dalton Trans.* **2010**, *39*, 1673−1688. (c) Ang, W. H.; Casini, A.; Sava, G.; Dyson, P. J. Organometallic ruthenium-based antitumor compounds with novel modes of action. *J. Organomet. Chem.* **2011**, *696*, 989−998. (d) Bergamo, A.; Gaiddon, C.; Schellens, J. H.; Beijnen, J. H.; Sava, G. Approaching tumour therapy beyond platinum drugs: Status of the art and perspectives of ruthenium drug candidates. *J. Inorg. Biochem.* **2012**, *106*, 90−99. (e) Ali, I.; Saleem, K.; Wesselinova, D.; Haque, A. DNA binding, hemolytic and anticancer assays of curcumin I based ligands and their ruthenium (III) complexes. *Med. Chem. Res.* **2013**, *22*, 1386−1398. (f) Ali, I.; Wani, W. A.; Saleem, K.; Wesselinova, D. Syntheses, DNA binding and anticancer profiles of L-Glutamic acid ligand and its copper(II) and ruthenium(III) complexes. *Med. Chem.* **2013**, *9*, 11−21.

(5) (a) Sava, G.; Zorzet, S.; Turrin, C.; Vita, F.; Soranzo, M.; Zabucchi, G.; Cocchietto, M.; Bergamo, A.; Di Giovine, S.; Pezzoni, G.; Sartor, L.; Garbisa, S. Dual Action of NAMI-A in inhibition of solid tumor metastasis: selective targeting of metastatic cells and binding to collagen. *Clin. Cancer Res.* **2003**, *9*, 1898−1905. (b) Pacor, S.; Zorzet, S.; Cocchietto, M.; Bacac, M.; Vadori, M.; Turrin, C.; Gava, B.; Castellarin, A.; Sava, G. Intratumoral NAMI-A treatment triggers metastasis reduction, which correlates to CD44 regulation and tumor infiltrating lymphocyte recruitment. *J. Pharmacol. Exp. Ther.* **2004**, *310*, 737−744.

(6) (a) Hartinger, C. G.; Zorbas-Seifried, S.; Jakupec, M. A.; Kynast, B.; Zorbas, H.; Keppler, B. K. From bench to bedside-preclinical and early clinical development of the anticancer agent indazolium trans-[tetrachlorobis(1H-indazole)ruthenate(III)] (KP1019 or FFC14A). *J. Inorg. Biochem.* **2006**, *100*, 891−904. (b) Hartinger, C. G.; Jakupec, M. A.; Zorbas-Seifried, S.; Groessl, M.; Egger, A.; Berger, W.; Zorbas, H.; Dyson, P. J.; Keppler, B. K. KP1019, a new redox-active anticancer agent-preclinical development and results of a clinical phase I study in tumor patients. *Chem. Biodivers.* **2008**, *5*, 2140−2155.

(7) (a) Ang, W. H.; Dyson, P. J. Classical and non-classical ruthenium-based anticancer drugs: Towards targeted chemotherapy. *Eur. J. Inorg. Chem.* **2006**, 4003−4018. (b) Dyson, P. J. Systematic design of a targeted organometallic antitumor drug in pre-clinical development. *Chimia* **2007**, *61*, 698−703. (c) Ang, W. H. Development of organometallic ruthenium(II) anticancer (RAPTA) drugs. *Chimia* **2007**, *61*, 140−142.

(8) (a) Peacock, A. F. A.; Sadler, P. J. Medicinal organometallic chemistry: Designing metal arene complexes as anticancer agents. *Chem.−Asian J.* **2008**, *3*, 1890−1899. (b) Dougan, S. J.; Sadler, P. J. The design of organometallic ruthenium arene anticancer agents. *Chimia* **2007**, *61*, 704−715. (c) Yan, K.; Melchart, M.; Habtemariam, A.; Sadler, P. J. Organometallic chemistry, biology and medicine: ruthenium arene anticancer complexes. *Chem. Commun.* **2005**, 4764−4776.

(9) Melchart, M.; Sadler, P. J. Ruthenium arene anticancer complexes. In *Bioorganometallics: Biomolecules, Labeling, Medicine*; Jaouen, G., Ed.; Wiley-VCH Verlag GmbH & Co. KGaA: Weinheim, 2006; pp 39−64.

(10) (a) Morris, R. E.; Aird, R. E.; Murdoch, P.; del, S.; Chen, H.; Cummings, J.; Hughes, N. D.; Parsons, S.; Parkin, A.; Boyd, G.; Jodrell, D. I.; Sadler, P. J. Inhibition of cancer cell growth by ruthenium(II) arene complexes. *J. Med. Chem.* **2001**, *44*, 3616−3621. (b) Aird, R. E.; Cummings, J.; Ritchie, A. A.; Muir, M.; Morris, R. E.; Chen, H.; Sadler, P. J.; Jodrell, D. I. In vitro and in vivo activity and cross resistance profiles of novel ruthenium (II) organometallic arene complexes in human ovarian cancer. *Br. J. Cancer* **2002**, *86*, 1652−1657.

(11) (a) Fernandez, R.; Melchart, M.; Habtemariam, A.; Parsons, S.; Sadler, P. J. Use of chelating ligands to tune the reactive site of half-sandwich ruthenium(II)−arene anticancer complexes. *Chem.—Eur. J.* **2004**, *10*, 5173−5179. (b) Habtemariam, A.; Melchart, M.; Fernandez, R.; Parsons, S.; Oswald, I. D.; Parkin, A.; Fabbiani, F. P.; Davidson, J. E.; Dawson, A.; Aird, R. E.; Jodrell, D. I.; Sadler, P. J. Structure−activity relationships for cytotoxic ruthenium(II) arene complexes containing N,N-, N,O-, and O,O-chelating ligands. *J. Med. Chem.* **2006**, *49*, 6858−6868.

(12) Scolaro, C.; Bergamo, A.; Brescacin, L.; Delfino, R.; Cocchietto, M.; Laurenczy, G.; Geldbach, T. J.; Sava, G.; Dyson, P. J. In vitro and in vivo evaluation of ruthenium(II)−arene PTA complexes. *J. Med. Chem.* **2005**, *48*, 4161−4171.

(13) Marchetti, F.; Pettinari, C.; Pettinari, R.; Cerquetella, A.; Cingolani, A.; Chan, E. J.; Kozawa, K.; Skelton, B. W.; White, A. H.; Wanke, R.; Kuznetsov, M. L.; Martins, L. M. D. R. S.; Pombeiro, A. J. L. Arene ruthenium(II) 4-Acyl-5-pyrazolonate derivatives: coordination chemistry, redox properties, and reactivity. *Inorg. Chem.* **2007**, *46*, 8245−8257.

(14) Marchetti, F.; Pettinari, C.; Pettinari, R. Acylpyrazolone ligands: Synthesis, structures, metal coordination chemistry and applications. *Coord. Chem. Rev.* **2005**, *249*, 2909−2945.

(15) Pettinari, C.; Pettinari, R.; Fianchini, M.; Marchetti, F.; Skelton, B. W.; White, A. H. Syntheses, structures, and reactivity of new pentamethylcyclopentadienyl-rhodium(III) and -iridium(III) 4-acyl-5-pyrazolonate complexes. *Inorg. Chem.* **2005**, *44*, 7933−7942.

(16) Geary, W. J. The use of conductivity measurements in organic solvents for the characterization of coordination compounds. *Coord. Chem. Rev.* **1971**, *7*, 81−122.

(17) (a) Kruck, T. Trifluorophosphinecomplexes of transition metals. *Angew. Chem., Int. Ed. Engl.* **1967**, *6*, 53−67. (b) Collong, W.; Kruck, T. Metal trifluorophosphine complexes. Hexakis(trifluorophosphine)-vanadium(0) synthesis, chemical properties, and reactions. *Chem. Ber.* **1990**, *123*, 1655−1656.

(18) Tardito, S.; Isella, C.; Medico, E.; Marchiò, L.; Bevilacqua, E.; Hatzoglou, M.; Bussolati, O.; Franchi-Gazzola, R. The thioxotriazole copper(II) complex A0 induces endoplasmic reticulum stress and paraptotic death in human cancer cells. *J. Biol. Chem.* **2009**, *284*, 24306−24319.

(19) Volarevic, V.; Vujic, J. M.; Milovanovic, M.; Kanjevac, T.; Volarevic, A.; Trifunovic, S. R.; Arsenijevic, N. Cytotoxic effects of palladium (II) and platinum (II) complexes with O,O′-dialkyl esters of (S,S)-ethylenediamine-N,N′-di-2-(4-methyl) pentanoic acid on human colon cancer cell lines. *J. BUON* **2013**, *18*, 131−137.

(20) Boulares, A. H.; Yakovlev, A. G.; Ivanova, V.; Stoica, B. A.; Wang, G.; Iyer, S.; Smulson, M. Role of poly(ADP-ribose) polymerase (PARP) cleavage in apoptosis. Caspase 3-resistant PARP mutant increases rates of apoptosis in transfected cells. *J. Biol. Chem.* **1999**, *274*, 22932−22940.

(21) Levine, A. J.; Momand, J.; Finlay, C. A. The p53 tumour suppressor gene. *Nature* **1991**, *351*, 453−456.

(22) Reed, J. C. Bcl-2 and the regulation of programmed cell death. *J. Cell. Biol.* **1994**, *124*, 1−6.

(23) Bevington, P. R.; Robinson, D. K. *Data Reduction and Error Analysis for the Physical Sciences*; McGraw-Hill: New York, 1992.

(24) Sheldrick, G. M. A short history of *SHELX*. *Acta Crystallogr., Sect. A: Found. Crystallogr.* **2008**, *64*, 112−122.
(25) Mosmann, T. J. Rapid colorimetric assay for cellular growth and survival: application to proliferation and cytotoxicity assays. *Immunol. Methods* **1983**, *65*, 55−63.
(26) Bradford, M. M. A rapid and sensitive method for quantitation of microgram quantities of protein utilizing the principle of protein-dye-binding. *Anal. Biochem.* **1976**, *72*, 248−254.
(27) Buonanno, F.; Quassinti, L.; Bramucci, M.; Amantini, C.; Lucciarini, R.; Santoni, G.; Iio, H.; Ortenzi, C. *Chem.-Biol. Interact.* **2008**, *176*, 151−164.
(28) Amici, M.; Bonfili, L.; Spina, M.; Cecarini, V.; Calzuola, I.; Marsili, V.; Angeletti, M.; Fioretti, E.; Tacconi, R.; Gianfranceschi, G. L.; Eleuteri, A. M. Wheat sprout extract induces changes on 20S proteasomes functionality. *Biochimie* **2008**, *90*, 790−801.
(29) Davies, R. J.; Edwards, P. R.; Watts, H. J.; Lowe, C. R.; Buckle, P. E.; Yeung, D.; Kinning, T. M.; Pollard-Knight, D. V. The resonant mirror: A versatile tool for the study of biomolecular interaction. In *Techniques in Protein Chemistry V*; Crabb, J. W., Ed.; Academic Press: San Diego, 1994; pp 285−292.
(30) Eriksson, S.; Kim, S. K.; Kubista, M.; Nordén, B. Binding of 4′,6-diamidino-2-phenylindole (DAPI) to AT regions of DNA: Evidence for an allosteric conformational change. *Biochemistry* **1993**, *32*, 2987−2998.
(31) Burres, N. S.; Frigo, A.; Rasmussen, R. R.; Mc Alpine, J. B. A colorimetric microassay for the detection of agents that interact with DNA. *J. Nat. Prod.* **1992**, *55*, 1582−1587.
(32) Le Pecq, J. B.; Paoletti, C. A fluorescent complex between ethidium bromide and nucleic acids. Physical-chemical characterization. *J. Mol. Biol.* **1967**, *27*, 87−106.